*Inorg. Chem.* **2007**, *46*, 4483–4491

Inorganic Chemistry
Article

# Copper-Linked Hexaniobate Lindqvist Clusters—Variations on a Theme

**Ranko P. Bontchev,† Eugene L. Venturini, and May Nyman***

*Sandia National Laboratories, P.O. Box 5800, MS 0754, Albuquerque, New Mexico 87185*

Received December 15, 2006

Four new one-dimensional materials and one dimer complex based on the linkage of $[Nb_6O_{19}]$ clusters and $[CuL_x]$ (L = ethylenediamine (en), $NH_3$, $H_2O$) assemble under ambient conditions. These phases include the following: $Rb_4[Cu(en)_2(H_2O)_2]_3[(Nb_6O_{19}H_2)_2Cu(en)_2]\cdot 24H_2O$ (**1**), space group $P\bar{1}$; $[Cu(en)_2(H_2O)_2]_2[(Nb_6O_{19}H_2)Cu(en)_2]\cdot 14H_2O$ (**2**), space group $P\bar{1}$; $Rb_2[Cu(NH_3)_2(H_2O)_4][Cu(NH_3)_4(H_2O)_2]_2\{[Nb_6O_{19}][Cu(NH_3)_2]_2\}_2\cdot 6H_2O$ (**3**), space group $P\bar{1}$; $\{[Nb_6O_{19}][Cu(NH_3)_2(H_2O)]_2[Cu(H_2O)_4]_2\}\cdot 3H_2O$ (**4**), space group *P2/n*; and $\{[Nb_6O_{19}][Cu(NH_3)_2(H_2O)]_2[Cu(H_2O)_4]_2\}$ (**5**), space group *C2/m*. All structures have been solved by single-crystal methods, and compounds **1**–**5** were characterized by thermogravimetric analysis, Fourier transform IR, chemical analysis, and magnetic measurements. It has been demonstrated that the conformation, charge, and geometry of the $[Nb_6O_{19}]$–$[CuL_x]$ chains can be modulated by varying the type and amount of the $[CuL_x]^{2+}$ species. The charge balance is provided by mixed $Rb^+/[CuL_x]^{2+}$ or $[CuL_x]^{2+}$ cations only for structures **1**–**3**, whereas **4** and **5** are neutral chains with no counterions. There are weak antiferromagnetic $Cu^{2+}$–$Cu^{2+}$ interactions in all phases. Compounds **2**–**5** represent the first examples in which the $[Nb_6O_{19}]$ Lindqvist ion forms extended solids rather than dimers or decorated monomers when reacted with transition-metal, cationic complexes.

## Introduction

Polyoxometalates, discrete anionic metal-oxo clusters, can be linked together through cationic moieties to build materials with incredible structural diversity, complexity, and functionality that are related to their form and composition. This strategy for controlled assembly of materials has been demonstrated by phases featuring linked polyoxovanadate, -molybdate, and -tungstate clusters.[1] With recent advances, we have learned that polyoxoniobate clusters also commonly self-assemble into framework solids composed of cluster anions interconnected by cations or polycations.[2] This is especially true of the dodecaniobate Keggin ion, $[XNb_{12}O_{40}]^{y-}$ (X = Si, Ge, P; $y$ = 15, 16).[2] Surprisingly, the Lindqvist hexaniobate ion[3] $[Nb_6O_{19}]^{8-}$ has never been similarly assembled into a framework solid, despite the fact that this cluster geometry is the most readily synthesized and manipulated among polyoxoniobates. Rather, decorated Lindqvist monomers or dimers have been obtained from reactions of $[Nb_6O_{19}]$ salts with transition-metal complexes. Examples of these are also scarce and include dimers $Na_{12}Mn[Nb_6O_{19}]_2\cdot 48H_2O$ and $K_8Na_4Ni[Nb_6O_{19}]_2\cdot 21H_2O$[4a] and monomers decorated with $Mn(CO)_3^+$, $Re(CO)_3^+$,[4b] or Ni(taci)$_2$ (taci = 1,3,5-triamino-1,3,5-trideoxy-cis-inositol).[4c]

The challenge in producing transition-metal-linked polyoxoniobates is retaining the transition-metal complex in solution under the alkaline conditions required for stabilization of polyoxoniobates. In the case of the linked Keggin ion materials,[2] base-soluble metals Ti and Nb served as the cationic linkers, and hydrothermal processing conditions

* To whom correspondence should be addressed. E-mail: mdnyman@sandia.gov.

† Present address: Cabot Corporation, 5401 Venice Ave. N.E. Albuquerque, NM 87113.

(1) (a) Khan, M. I. *J. Solid State Chem.* **2000**, *152*, 105. (b) Khan, M. I.; Yohannes, E.; Powell, D. *Inorg. Chem.* **1999**, *38*, 212. (c) Khan, M. I.; Yohannes, E.; Powell, D. *Chem. Commun.* **1999**, 23. (d) Hagrman, P. J.; Hagrman, D.; Zubieta, J. *Angew. Chem., Int. Ed.* **1999**, *38*, 2639. (e) Lu, J.; Xu, Y.; Goh, N. K. L. S.; Chia, L. S. *Chem. Commun.* **1999**, 832. (f) Do, J.; Bontchev, R. P.; Jacobson, A. J. *Inorg. Chem.* **2000**, *39*, 4305. (g) Reinoso, S.; Vitoria, P.; Gutierrez-Zorrilla, J. M.; Lezama, L.; San Felices, L.; Beitia, J. I. *Inorg. Chem.* **2005**, *44*, 9731. (h) Long, D. L.; Kogerler, P.; Farrugia, L. J.; Cronin, L. *Dalton Trans.* **2005**, *8*, 1372. (i) Mialane, P.; Dolbecq, A.; Secheresse, F. *Chem. Commun.* **2006**, *33*, 3477. (j) Lu, Y.; Xu, Y.; Li, Y. G.; Wang, E. B.; Xu, X. X.; Ma, Y. *Inorg. Chem.* **2006**, *45*, 2055.

(2) (a) Nyman, M.; Bonhomme, F.; Alam, T. M.; Rodriguez, M. A.; Cherry, B. R.; Krumhansl, J. L.; Nenoff, T. M. A. M.; Sattler, A. M. *Science* **2002**, *297*, 996. (b) Bonhomme, F.; Larentzos, J. P.; Alam, T. M.; Maginn, E. J.; Nyman, M. *Inorg. Chem.* **2005**, *44*, 1774. (c) Nyman, M.; Celestian, A. J.; Parise, J. B.; Holland, G. P.; Alam, T. M. *Inorg. Chem.* **2006**, *45*, 1043. (d) Nyman, M.; Larentzos, J. P.; Maginn, E. J.; Welk, M. E.; Ingersoll, D.; Park, H.; Parise, J. B.; Bull, I.; Bonhomme, F. *Inorg. Chem.* **2007**, *46*, 2067−2079.

(3) Lindqvist, I. *Ark. Kemi.* **1953**, *5*, 247.

(4) (a) Flynn, C.; Stucky, G. *Inorg. Chem.* **1969**, *8*, 332. (b) Besserguenev, A.; Dickman, M.; Pope, M. *Inorg. Chem.* **2001**, *40*, 2582. (c) Hegetschweiler, K.; Finn, R.; Rarig, R.; Sander, J.; Steinhauser, S.; Worle, M.; Zubieta, J. *Inorg. Chim. Acta* **2002**, *337*, 39.

10.1021/ic0624118 CCC: $37.00 
Published on Web 05/02/2007

probably also favored the formation of framework solids containing intact clusters. Zubieta et al. used the strategy of large chelating ligands such as "taci"[4c] for maintaining transition-metal solubility, but this limits the possibility of propagating infinite solids. When devising strategies for forming linked-cluster solids, we also need to take into consideration the bonding geometry of the transition-metal cations to the Lindqvist ion. In all of the above-mentioned structures featuring Lindqvist ions and transition metals, the transition metal is $\mu_3$ bonded to a face of the $[Nb_6O_{19}]$ superoctahedron. This is also a commonly observed bonding geometry for alkalis.[5] In the case of the Mn and Ni dimers, the transition-metal octahedron is sandwiched between and face-sharing with two Lindqvist ions.[4a]

This raises the question of why a chain of alternating Lindqvist ions and transition-metal octahedra cannot be propagated. With the use of the $Mn[Nb_6O_{19}]_2$ complex as an example, the $MnO_6$ octahedron (where the oxygens are the $\mu_2$-$O_b$ (b = bridging) oxygens of the cluster) is very regular, with $Mn-O_b$ bond distances ranging from 1.86 to 1.88 Å.[4a] On the other hand, the $[Nb_6O_{19}]$ cluster becomes distorted with the lengthening of the Mn-associated $Nb-O_b$ bonds and corresponding shortening of the trans $Nb-O_b$ bonds. From this observation, one might surmise that the distortion of the cluster as a result of face-sharing with a single $TM(O)_6$ (TM = transition metal) octahedron does not allow for similar bonding to a second transition metal. Additionally, the proposed one-dimensional chain of alternating $[Nb_6O_{19}]$ superoctahedra and $TM(O)_6$ octahedra would be extremely rigid, and perhaps such a chain would not allow the flexibility required for chain-packing or the accommodation of lattice water and counterions.

On the other hand, the Jahn−Teller character of the d-9 $Cu^{2+}$ atom favors asymmetric coordination, and therefore, alternative types of bonding might be expected, for example, axial linkage instead of face-sharing with Lindqvist ions. This strategy has also been used successfully by Zubieta et al. for the linkage of polyoxomolybdate clusters.[5] Furthermore, the $Cu^{2+}$ ion can be stabilized in alkaline solutions with coordinating amine ligands. In this study, we present the synthesis, structural characterization, and magnetic measurements of the first examples of one-dimensional materials composed of $[Nb_6O_{19}]$ clusters linked by transition-metal complexes. Four examples of one-dimensional materials are described, along with a dimer complex, thus extending the structural diversity of linked polyoxoniobate materials.

## Experimental Section

**Synthesis**. The title compounds **1**−**5** have been synthesized following similar procedures. Generally, an aqueous solution of the ligand ($NH_3$, en; en = ethylenediamine) was added to an aqueous solution of $Cu(NO_3)_2{\cdot}2.5H_2O$ while stirring at room temperature. The resulting deep blue or purple solution was added dropwise to a beaker containing an aqueous solution of $[Rb_8Nb_6O_{19}]{\cdot}14H_2O$. The $[Rb_8Nb_6O_{19}]{\cdot}14H_2O$ was prepared as described previously.[6] This solution was stirred at 60 °C for 2 h and left at room temperature for 3 to 5 days for crystallization. Details are as follows: **1**, 4.00 g $Rb_8Nb_6O_{19}{\cdot}14H_2O$ (2.2 mmol), 2.00 g $Cu(NO_3)_2{\cdot}2.5H_2O$ (8.6 mmol), 20 mL ethylenediamine (300 mmol), 80 mL $H_2O$ (4400 mmol); **2**, 2.00 g $Rb_8Nb_6O_{19}{\cdot}14H_2O$ (1.1 mmol), 2.00 g $Cu(NO_3)_2{\cdot}2.5H_2O$ (8.6 mmol), 20 mL ethylenediamine (300 mmol), 80 mL $H_2O$ (4400 mmol); **3**, 0.90 g $Rb_8Nb_6O_{19}{\cdot}14H_2O$ (0.6 mmol), 0.48 g $Cu(NO_3)_2{\cdot}2.5H_2O$ (2 mmol), 2 mL 28% $NH_4OH$ (30 mmol), 16 mL $H_2O$ (900 mmol); **4** and **5**, 0.80 g $Rb_8Nb_6O_{19}{\cdot}14H_2O$ (0.6 mmol), 0.50 g $Cu(NO_3)_2{\cdot}2.5H_2O$ (2 mmol), 20 mL 28% $NH_4OH$ (300 mmol), 60 mL $H_2O$ (3300 mmol). The syntheses of **1**−**3** resulted in single-phase products confirmed by a comparison of their experimental powder X-ray diffraction (XRD) patterns with the simulated ones based on the crystal structures refinement data.[7d] Compounds **4** and **5** crystallized upon the same reaction conditions and in the same beaker; due to their high air sensitivity the relative yields were visually estimated from the mixed crystal batch.

Yields based on copper (wt %): **1**, 90; **2**, 80; **3**, 85; **4**, 30; **5**, 25. After 3−5 days, a crystalline product formed at the bottom of each beaker. In some cases (**1**−**3**), a small addition of MeOH after the first day improved the crystallinity of the products. After being filtered and washed with the minimum amount of MeOH, the crystals were stored in sealed vials for further analyses. Compounds **4** and **5** crystallized from the same batch. These phases are extremely sensitive and quickly decay when exposed to air or moisture. For that reason, they were not filtered but rather were stored in the mother liquor. Crystals of **4** and **5** selected for single-crystal XRD studies were quickly transferred and sealed into small vials containing Paratone-N.

Chemical analyses were performed by Galbraith Laboratories, Inc. (wt %, calculated/found): **1**, Nb 33.33/31.7, Cu 7.6/7.2, N 6.7/7/7, H 3.2/3.8, C 5.8/6/4; **2**, Nb 33.4/31.8, Cu 11.3/11.3, N 10.1/10.9, H 4.4/4.9, C 10.3/10.0; **3**, Nb 39.4/36.7, Cu 15.7/16.0, N 6.9/7.0, H 2.5/2.7; **4**, Nb 36.0/35.9, Cu 15.5/15.5, N 6.9/5.8, H 2.9/2.2; **5**, Nb 39.3/40.5, Cu 17.9/17.7, N 3.9/3.8, H 2.7/2.5.

**X-ray Crystallography.** The crystal structures of compounds **1**−**5** were solved by single-crystal XRD methods. For each crystal, a hemisphere of data was collected at 293 K using a Siemens SMART 1K CCD diffractometer (Mo Kα radiation, $\lambda$ = 0.71073 Å, graphite monochromator, narrow-frame scan). The program *SADABS*[7a] was used for the absorption correction. The structures were solved by direct methods and refined by least-squares methods on $F^2$ using the *SHELX97*[7b] software package. The main crystallographic data and interatomic distances for **1**−**5** are listed in Table 1 and Table 2, respectively. Full crystallographic information is provided in the Supporting Information in CIF format. Initially, all metal (Nb, Cu, Rb) and oxygen atoms belonging to the Lindqvist clusters were located. Next, the carbon, nitrogen, and oxygen atoms of en, $NH_3$, and $H_2O$ were located and assigned with the help of the chemical, magnetic, and thermogravimetric (TGA) analyses.

(5) (a) Zapf, P. J.; Hagrman, D.; Zubieta, J. *Comments Inorg. Chem*. **1999**, *21*, 225. (b) Burkholder, E.; Golub, V.; O-Connor, C.J.; Zubieta, J. *Inorg. Chem*. **2004**, *43*, 7014. (c) Hagrman, D.; Hagrman, P.; Zubieta, J. *Inorg. Chim. Acta* **2000**, *300*, 212.

(6) Nyman, M.; Alam, T.; Bonhomme, F.; Rodriguez, M.; Frazer, C.; Welk, M. *J. Cluster Sci*. **2006**, *17*, 197.

(7) (a) Sheldrick, G. M. *SADABS*, *Program for Empirical Absorption Correction of Area Detector Data*, version 2.10; University of Gottingen: Gottingen, Germany, 2003. (b) *SHELX97* (Includes *SHELXS97*, *SHELXL97*, and *CIFTAB*), *Programs for Crystal Structure Analysis*, release 97-2; Institüt für Anorganische Chemie der Universität: Göttingen, Germany, 1998. (c) Spek, A. L. *Acta Crystallogr*., *Sect. A* **1990**, *C34*, 46−57. (d) Spek, A. L. *PLATON, A Multipurpose Crystallographic Tool*; Utrecht University: Utrecht, The Netherlands, 1998.

**Table 1.** Crystal Data and Structure Refinement Parameters for **1**−**5**

| | compound | | | | |
|---|---|---|---|---|---|
| | **1** | **2** | **3** | **4** | **5** |
| formula | $C_8H_{53}Cu_2N_8Nb_6O_{34}Rb_2$ | $C_{12}H_{74}Cu_3N_{12}Nb_6O_{33}$ | $Cu_{3.5}H_{35}N_7Nb_6O_{31}Rb$ | $Cu_4H_{42}N_4Nb_6O_{34}$ | $Cu_4H_{32}N_4Nb_6O_{29}$ |
| $M$ (g) | 1661.06 | 1664.5 | 1494.4 | 1453.6 | 1363.2 |
| $T$ (K) | 293(2) | 293(2) | 293(2) | 293(2) | 293(2) |
| $\lambda$ (Å) | 0.71073 | 0.71073 | 0.71073 | 0.49594 | 0.71073 |
| cryst syst | triclinic | triclinic | triclinic | monoclinic | monoclinic |
| space group | $P\bar{1}$ (No. 2) | $P\bar{1}$ (No. 2) | $P\bar{1}$ (No. 2) | $P2/n$ (No. 13) | $C2/m$ (No. 12) |
| $a$ (Å) | 11.9708(13) | 12.6242(10) | 8.7520(7) | 13.6592(11) | 18.266(5) |
| $b$ (Å) | 12.3451(13) | 12.6577(10) | 13.0771(10) | 8.8725(7) | 8.913(5) |
| $c$ (Å) | 17.4481(19) | 16.4412(13) | 15.9280(13) | 13.8676(10) | 13.591(5) |
| α (deg) | 88.9170(10) | 74.6220(10) | 86.6190(10) | 90.00 | 90.00 |
| $\beta$ (deg) | 89.4450(10) | 88.5410(10) | 83.6490(10) | 96.446(3) | 130.840(5) |
| $\gamma$ (deg) | 61.6010(10) | 81.5020(10) | 88.0440(10) | 90.00 | 90.00 |
| $V$ (Å$^3$) | 2267.8(4) | 2505.1(3) | 1807.9(2) | 1670.0(2) | 1674.0(1) |
| $Z$ | 2 | 2 | 2 | 2 | 2 |
| calc $\rho$ (g/cm$^3$) | 2.433 | 2.207 | 2.681 | 2.807 | 2.737 |
| $\mu$ (mm$^{-1}$) | 4.615 | 2.668 | 5.283 | 8.003 | 4.566 |
| $F$(000) | 1614 | 1656 | 1363 | 1324 | 1292 |
| $\theta$ range (deg) | 1.93 to 26.03 | 1.28 to 23.00 | 1.29 to 22.50 | 1.60 to 19.28 | 1.98 to 23.50 |
| $hkl$ range | $-14 \le h \le 14$<br>$-14 \le k \le 15$<br>$-21 \le l \le 21$ | $-13 \le h \le 13$<br>$-13 \le k \le 13$<br>$-18 \le l \le 18$ | $9 \le h \le 9$<br>$-14 \le k \le 14$<br>$-17 \le l \le 17$ | $-18 \le h \le 18$<br>$0 \le k \le 11$<br>$0 \le l \le 18$ | $-20 \le h \le 20$<br>$-10 \le k \le 10$<br>$-15 \le l \le 14$ |
| reflns/unique | 19886/8107 | 20557/6946 | 10620/4729 | 3748/3748 | 2840/1302 |
| data/params | 8107/754 | 6946/688 | 4729/452 | 3748/102 | 1302/127 |
| GOF on $F^2$ | 1.034 | 1.042 | 1.078 | 1.130 | 1.025 |
| R1 [$I > 2\sigma(I)$] | 0.0273 | 0.0245 | 0.0265 | 0.0904 | 0.0877 |
| wR2 [$I > 2\sigma(I)$] | 0.0671 | 0.0657 | 0.0719 | 0.1777 | 0.2236 |

**Table 2.** Main Interatomic Distances (Å) for 1−**5**

| A−X | **1** | **2** | **3** | **4** | **5** |
|---|---|---|---|---|---|
| Nb−O | 1.910(3)−2.151(3) | 1.900(3)−2.056(3) | 1.926(4)−2.059(4) | 1.942(11)−2.061(10) | 1.971(15)−2.007(16) |
| Nb−OH | 2.126(3)−2.151(3) | 2.140(3)−2.134(3) | N/A | N/A | N/A |
| Nb═O | 1.762(3)−1.795(3) | 1.757(3)−1.797(3) | 1.769(4)−1.787(4) | 1.776(12)−1.788(11) | 1.71(2)−1.76(2) |
| Nb−$O_{\mu_6}$ | 2.361(2)−2.437(2) | 2.320(3)−2.488(3) | 2.357(1)−2.388(1) | 2.361(9)−2.388(9) | 2.378(3)−2.378(2) |
| Cu−N | 2.001(4)−2.026(3) | 2.000(4)−2.019(4) | 1.972(4)−2.047(4) | 1.980(12)−1.993(12) | 1.96(3)−1.97(3) |
| Cu−$O_{Nb_6O_{19}}$ | 2.532(3) | 2.453(4)−2.673(4) | 1.918(4)−2.002(4) | 2.042(10)−2.358(10) | 2.158(16)−2.343(7) |
| Cu−$O_{H_2O}$ | 2.478(4)−2.849(5) | 2.524(4)−2.817(4) | 2.272(4)−2.671(4) | 2.286(12)−2.776(14) | 2.24(3)−2.63(3) |

Next, the thermal parameters of the above atoms were refined anisotropically. Finally, the hydrogen atoms were found directly from the Fourier maps (**1**−**3**) and their thermal parameters were refined isotropically. After the refinements converged, a careful examination of the solutions using the *PLATON* program[7c,d] confirmed the accuracy of the corresponding space groups and the lack of higher symmetry.

**Characterization**. Infrared spectra were recorded on a Perkin-Elmer Spectrum One spectrometer within the range of 400−4000 cm$^{-1}$ using the KBr pellet method. Thermogravimetric-differential thermal analysis (TGA-DTA) experiments were performed on a TA Instruments SDT Q600 analyzer with air as a carrier gas (100 cm$^3$/min) and a heating rate of 10 °C/min. The magnetic susceptibility of **1**−**5** was measured from 300 to 5 K in an applied field of 10 mT using a commercial superconducting quantum interference device magnetometer (Quantum Design, San Diego, CA, model MPMS-7). The molar susceptibility $\chi_m$ of each powder sample was calculated from the measured weight using the XRD and chemical analyses information. The data were fit to three adjustable parameters using a Curie−Weiss law $\chi_m = A + C/(T + \theta)$, where $A$ is a temperature-independent constant, $C$ is the Curie constant arising from the Cu(II) paramagnetic ions, and $\theta$ is the paramagnetic Curie temperature reflecting the collective interactions among the magnetic ions.[8]

(8) Morrish, A. H. In *The Physical Principles of Magnetism*; John Wiley & Sons: New York, 1965; Chapter 6.

## Results

**Description of the Structures.** The crystal structures of compounds **1**−**5** can be generally described as Lindqvist [$Nb_6O_{19}$] clusters linked together by copper complexes of the type $CuL_x$ (L = en, $NH_3$, $H_2O$).

Structure **1** contains the negatively charged dumbbell dimers $\{[Nb_6O_{19}H_2]-Cu(en)_2-[Nb_6O_{19}H_2]\}^{10-}$ (Figure 1a). They are composed of two diprotonated $[Nb_6O_{19}H_2]^{6-}$ Lindqvist clusters linked by a $[Cu(en)_2]^{2+}$ complex. The linkage involves one bridging $O_b$ atom of each cluster with elongated Cu−$O_b$ distances of 2.532(4) Å, the Cu−N distances remaining well within the range reported for such complexes, 2.001(4) and 2.020(4) Å, respectively.[9,10] Hence, these dimers can also be simplistically described as two [$Nb_6O_{19}$] superoctahedra linked by a [$CuO_2N_4$] octahedron. Two protons are associated with each [$Nb_6O_{19}$] cluster and are attached to two neighboring bridging oxygen atoms. A very interesting detail, directly related to the structure of **2**, is the fact that these proton pairs are located in a trans orientation with respect to the central $[Cu(en)_2]^{2+}$ complex

(9) (a) Bontchev, R.; Nyman, M. *Angew. Chem., Int. Ed.* **2006**, *45*, 6670. (b) Bontchev, R.; Nyman, M. *Angew. Chem.* **2006**, *118*, 6822−6824.

(10) (a) Morosin, B. *Acta Crystallogr.* **1976**, *B32*, 1237. (b) Troyanov, S.; Morozov, I.; Znamenkov, K.; Korenev, Y. *Z. Anorg. Allg. Chem.* **1995**, *621*, 1261.

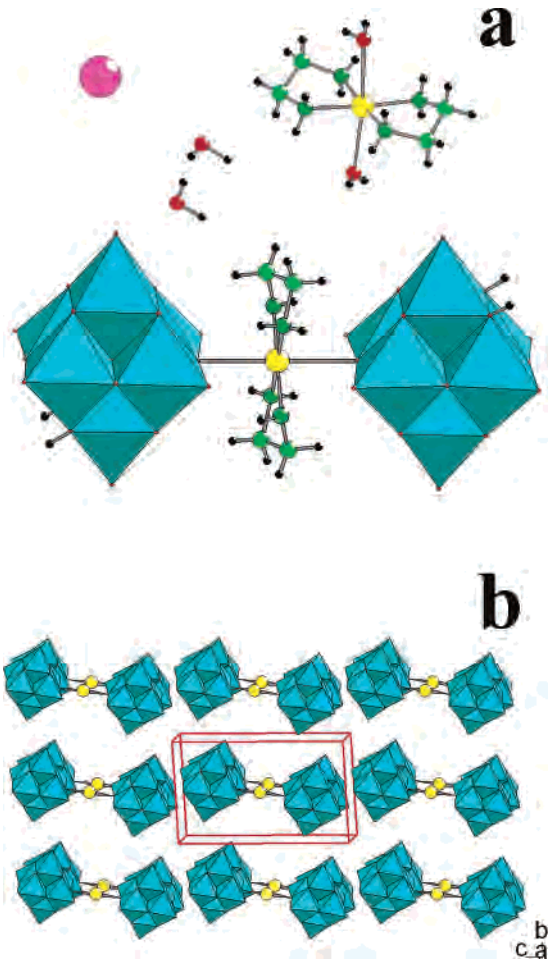


**Figure 1.** View of the structure of **1**: (a) building units and (b) packing of the $[Nb_6O_{19}H_2]-Cu-[Nb_6O_{19}H_2]$ dumbbell dimers and unit cell. Color key: $NbO_6$, cyan; Cu, yellow; Rb, purple; C, light green; N, dark green; O, red; H, black.

(Figure 1a). The $\{[Nb_6O_{19}H_2]-Cu(en)_2-[Nb_6O_{19}H_2]\}^{10-}$ dimers are arranged in layers parallel to the *ac* plane (Figure 1b). The protonated faces of adjacent dimers are associated through two $O_b-H\cdots O_b$ and two $O_b-H\cdots O_t$ hydrogen bonds, as observed previously in alkali $[H_2Nb_6O_{19}]$ salts.[6] The space between the layers is filled with water molecules and the charge-balancing $Rb^+$ and $[Cu(en)_2(H_2O)_2]^{2+}$ species.

The crystal structure of **2** is similar to that of **1** and can be considered an infinite extension of the dimers (Figure 2). The diprotonated $[Nb_6O_{19}H_2]^{6-}$ clusters and $[Cu(en)_2]^{2+}$ complexes are linked together in an alternating mode to form infinite zigzag $\{-[Nb_6O_{19}H_2]-Cu(en)_2-\}^{4-}$ negatively charged chains (Figure 2a). The topology and the trans-protonated sites in any $\{[Nb_6O_{19}H_2]-Cu(en)_2-[Nb_6O_{19}H_2]\}$ section of **2** are virtually identical to the dimers in **1**. To propagate further in the same fashion, the only sterically available sites for the next $[Cu(en)_2]^{2+}$ link in **2** are the two geometrically equivalent bridging $O_b$ atoms located on the opposite faces of the protonated ones in the $[Nb_6O_{19}H_2]$ clusters (Figure 2a). Hence, in each $\{[Nb_6O_{19}H_2]-Cu(en)_2-[Nb_6O_{19}H_2]\}$ section of **2**, the protonated sites remain in trans orientation with respect to each other, which in turn determines the zigzag shape of the chains. As in **1**, the chains can be described as alternating $[Nb_6O_{19}]$ superoctahedra and $[CuO_2N_4]$

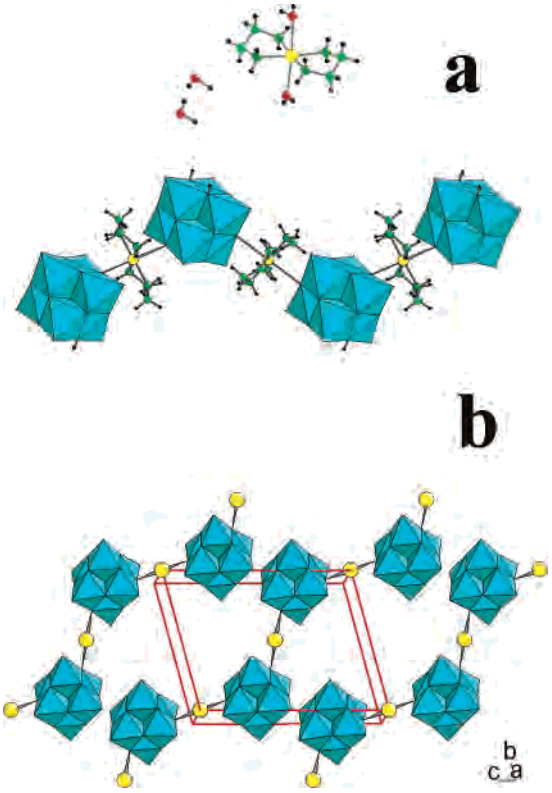


**Figure 2.** View of the structure of **2**: (a) building units and (b) packing of the zigzag $\{-[Nb_6O_{19}H_2]-Cu-\}$ chains and unit cell. Color key: $NbO_6$, cyan; Cu, yellow; C, light green; N, dark green; O, red; H, black.

octahedra. Another difference between **1** and **2** is the orientation of the neighboring $[Nb_6O_{19}H_2]$ clusters. The $[Nb_6O_{19}]$ superoctahedrons' four-fold axes in **1** are virtually parallel to each other (Figure 1a), whereas in **2** they are tilted at about 20° with respect to each other (Figure 2a). The two $Cu-O_b$ distances in **1** are equivalent, 2.532(4) Å, whereas in **2** the $Cu-O_b$ distances in every two alternating $\{-[Nb_6O_{19}H_2]-Cu(en)_2-[Nb_6O_{19}H_2]\}$ sections are 2.673(3) and 2.453(3) Å, respectively. Although the average of these lengths (2.563 Å) virtually matches that in **1**, there is no obvious explanation for this alternating bond-length difference of almost 0.2 Å. The zigzag chains are parallel and run along the [011] direction (Figure 2b). As in the structure of **1**, the protonated sites of the clusters face each other and direct the three-dimensional arrangement of the chains by forming a hydrogen-bonded network. The space between the chains is filled by water molecules and countercations. Different from that of **1**, however, the charge balance in **2** is provided solely by octahedral $[Cu(en)_2(H_2O)_2]^{2+}$ cations and there are no $Rb^+$ or any other metal cations in the structure (Figure 2a).

The most prominent feature in the structure of **3** is the straight $\{\cdots[Nb_6O_{19}]-[Cu(NH_3)]_2\cdots\}^{4-}$ chains (Figure 3a). In these chains, each two neighboring nonprotonated $[Nb_6O_{19}]^{8-}$ clusters are linked together by two $[Cu(NH_3)]^{2+}$ species on the same side of the cluster. The copper atoms are in typical square-planar coordination involving two bridging ($O_b$) atoms from one $[Nb_6O_{19}]$ cluster, one terminal ($O_t$) atom of another neighboring cluster, and a terminal $NH_3$, $[Cu(O_b)_2O_t(NH_3)]$. The main difference compared with **1** and

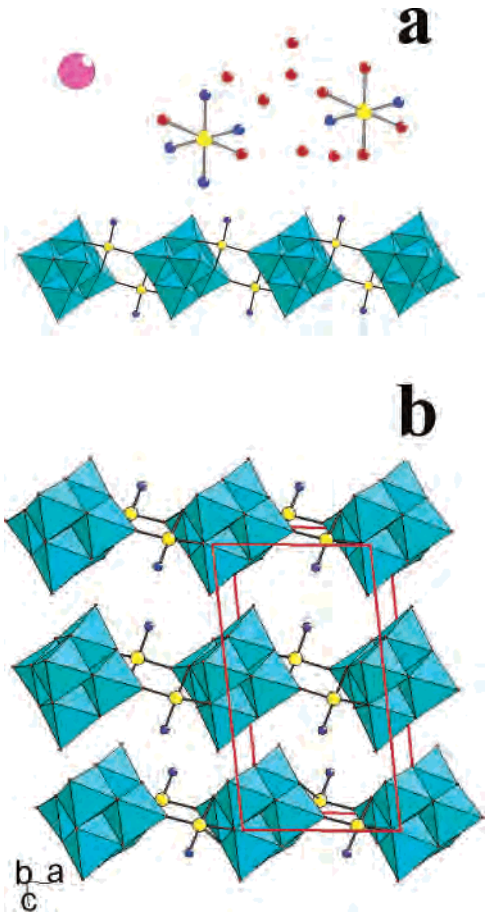


**Figure 3.** View of the structure of **3**: (a) building units and (b) packing of the straight $\{-[Nb_6O_{19}]-[Cu(NH_3)]_2-\}$ chains and unit cell. Color key: $NbO_6$, cyan; Cu, yellow; Rb, purple; N, blue; O, red.

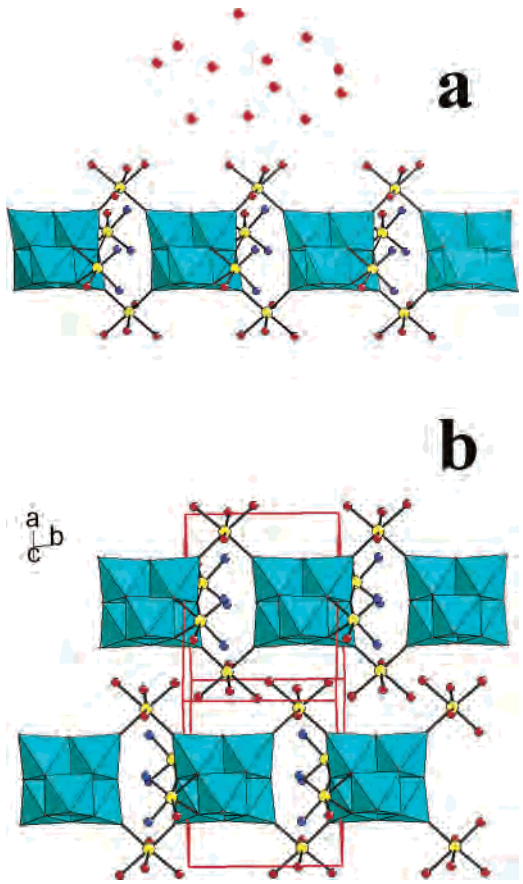


**Figure 4.** View of the structure of **4**: (a) building units and (b) packing of the straight $\{-[Nb_6O_{19}][Cu(NH_3)_2(H_2O)]_2-[Cu(H_2O)_4]_2-\}$ chains and unit cell. Color key: $NbO_6$, cyan; Cu, yellow; N, blue; O, red.

**2** is that in **3** the connectivity between the clusters is provided by two, rather than one copper atom, and each of these Cu atoms provides two Cu−$O_b$ bonds with a $[Nb_6O_{19}]$ cluster. The third Cu−$O_t$ bond has been previously observed in Cu-$(en)_2$-linked $[Nb_{24}O_{72}H_9]$.[9] As in **1**, the chains run along the *a* axis, forming layers parallel to the *ab* plane (Figure 3b). The space between the chains is filled with water molecules and countercations. In this case, however, the charge balance is provided by two different octahedral copper complexes, $[Cu(NH_3)_2(H_2O)_4]^{2+}$ and $[Cu(NH_3)_4(H_2O)_2]^{2+}$, together with the $Rb^+$ cations. The nitrogen and oxygen atoms of the $NH_3$− and $H_2O$ ligands have been assigned after a careful evaluation and combination of the data from the XRD, chemical, and TGA analyses. In general, Cu−L distances of close to 2.0 Å have been considered to indicate a Cu−$NH_3$ bond whereas those of 2.3 Å and above have been considered to indicate a Cu−$OH_2$ bond (Table 2).[9] After using this rule and assigning the corresponding occupied positions, the resulting "theoretical" sum of nitrogen atoms matched very well the data from the chemical analysis. The TGA data also provided supportive evidence, assuming that the water molecules (both space-filling and Cu-coordinated) are volatilized before the Cu-coordinated $NH_3$ (Supporting Information, Figure SI3).

The dominant feature of **4** is the straight $\{-[Nb_6O_{19}][Cu(NH_3)_2(H_2O)]_2-[Cu(H_2O)_4]_2-\}$ chains (Figure 4). Here, each set of two nonprotonated $[Nb_6O_{19}]$ clusters is linked together by two bridging octahedral $[Cu(H_2O)_4]$ complexes via terminal cluster $O_t$ oxygen atoms. Additionally, each $[Nb_6O_{19}]$ cluster is also "decorated" by two $[Cu(NH_3)_2(H_2O)]$ complexes (Figure 4a). These "decorating" copper atoms are in octahedral coordination, the remaining three ligands being three bridging $O_b$ atoms from the attached $[Nb_6O_{19}]$ cluster. As in the case of **3**, the N and O atoms have been assigned after careful analysis of the Cu−L interatomic distances and analytical and TGA data (Table 2.) The chains propagate parallel to the *b* axis (Figure 4b), and the interchain space is filled by loosely associated water molecules. In contrast to the previously discussed phases of **1**−**3**, the chains in **4** are neutral and no $Rb^+$ or $(CuL_6)^{2+}$ complexes are present as charge-compensating cations in the structure.

The structure of **5** is closely related to that of **4** (Figure 5a). In fact, it is the dehydrated form of the same compound, which explains the fact that **4** and **5** always form in a single reaction, under the same reaction conditions. The lack of templating water molecules in **5** accounts for the different overall crystal symmetry and space group (Table 1). This difference causes a positional disorder of the two decorating, nonbridging copper atoms in **5** among four different crystallographically equivalent sites (Figure 5b). Although it is not possible to distinguish the actual occupancy of these positions by X-ray analysis, our magnetic studies provided valuable insight on this topic and we are inclined to assume a preferential occupancy of the same sites as in **4** (vide

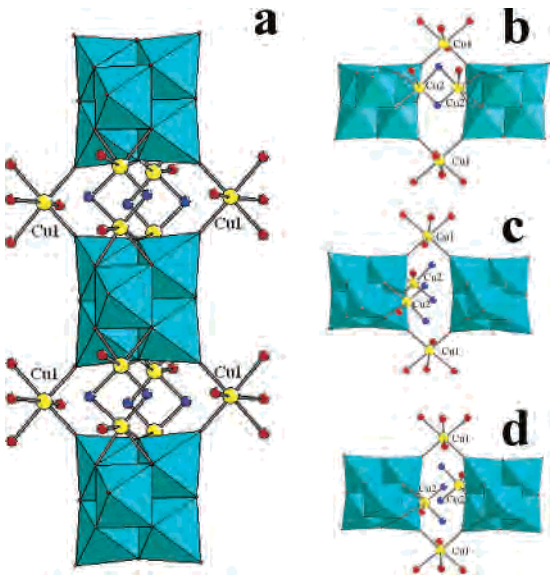


**Figure 5.** View of the structure of **5**: (a) $\{-[Nb_6O_{19}][Cu(NH_3)_2(H_2O)]_2-[Cu(H_2O)_4]_2-\}$ chains with the formal Cu2 positional disorder; (b−d) possible actual occupancy and orientation of the $Cu2(NH_3)_2(H_2O)O_3$ octahedra. Color key: $NbO_6$, cyan; Cu, yellow; N, blue; O, red.

supra). Visual observations as well as TGA studies indicate that the hydrated (**4**) and dehydrated (**5**) forms are in equilibrium and the water molecules could be easily removed or added even at room temperature, which explains the relatively poor quality of the crystals and their high sensitivity and reactivity.

Infrared spectra confirmed the presence of en and $NH_3$ in the structures (Supporting Information, Figure SI2. The strongest bands have been assigned[8,11] as follows: Nb−$O_b$ = 400−750 $cm^{-1}$; Nb═$O_t$ = 800−1100 $cm^{-1}$; en = 900−1450 and 2800−3300 $cm^{-1}$; $NH_3$ = 920, 1250, and 1550 $cm^{-1}$; $H_2O$ =1600 and 3300 $cm^{-1}$.

TGA data confirmed the compositions derived from XRD and chemical analyses. Both $[Cu(en)_2]$- (**1** and **2**) and $[Cu(NH_3)_x(H_2O)_y]$-linked compounds (**3**−**5**) show very similar behavior (Supporting Information, Figure SI3). Upon heating, they initially lose all water of crystallization in a single step from room temperature to about 180−200 °C. Next, they simultaneously lose the Cu-coordinated en, $NH_3$, and $H_2O$ at temperatures up to 350−400 °C. At the final stage, the remaining residues correspond to solids of nominal compositions $Rb_2O{\cdot}CuO{\cdot}Nb_2O_5$ (**1** and **3**) or $CuO{\cdot}Nb_2O_5$ (**2**, **4**, and **5**).

**Magnetic Measurements.** Initial attempts to fit the $\chi_m = f(T)$ data using the Curie law $\chi_m = A + C/T$ with only two variables ($A$ and $C$) led to unsatisfactory results. This indicated that, although weak, there are still some measurable magnetic interactions between the $Cu^{2+}$ species in the structures. Later fits using the Curie−Weiss law confirmed this assumption, yielding values of the $\theta$ parameters ranging between −0.4 and −7.1 K (Table 3and Figure 6). In **1**, the

(11) (a) Farell, F.; Maroni, V.; Spiro, T. *Inorg. Chem* **1969**, *8*, 2638. (b) Rocchiccioli, C.; Thouvenot, R.; Dabbabi, M. *Spectrochim. Acta* **1977**, *33A*, 143. (c) Nakamoto, K.; In *Infrared and Raman Spectroscopy of Inorganic and Coordination Compounds*, 5th ed.; John Wiley & Sons: New York, 1997.

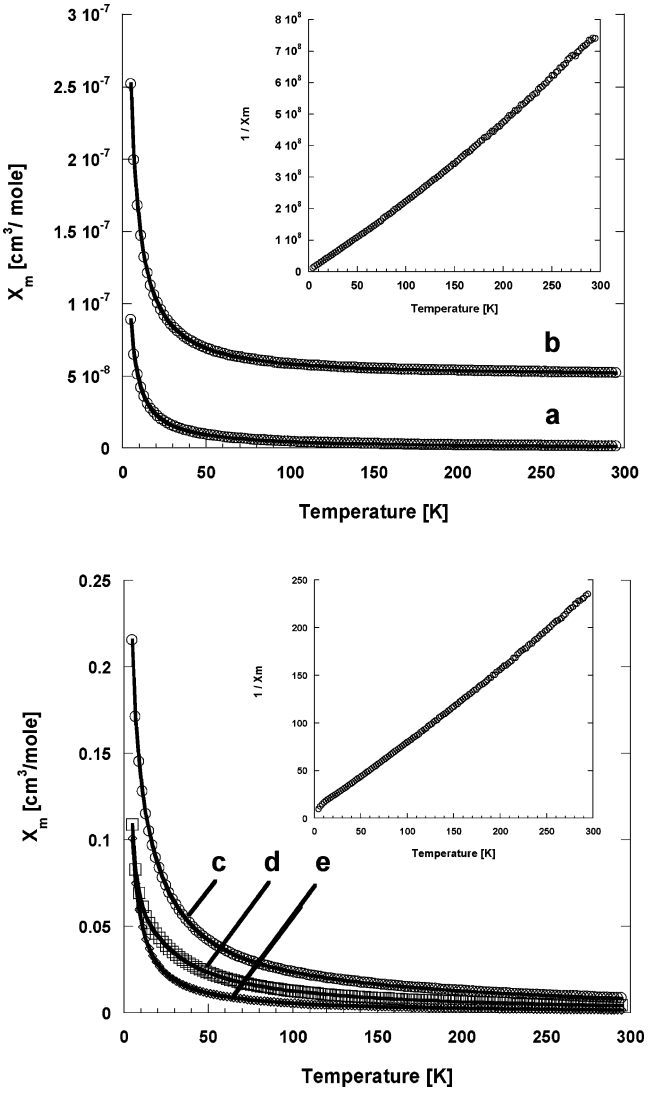


**Figure 6.** Variation of the molar magnetic susceptibility $\chi_m$ as a function of temperature; experimental data and fits are shown as open figures and solid lines, respectively. Top: **1** (a), **2** (b), and inset $1/\chi_m(T)$ for **1**. Bottom: **3** (c), **4** (e), **5** (d), and inset $1/\chi_m(T)$ for **3**.

only possible $Cu^{2+}-Cu^{2+}$ interactions could take place between the bridging $Cu_b$ atoms from the $[(Nb_6O_{19})-Cu-(Nb_6O_{19})]$ dimers ($Cu_b-Cu_b$), between the bridging $Cu_b$ and isolated $Cu_i$ atoms in $[Cu(en)_2(H_2O)_2]$ ($Cu_b-Cu_i$), and between the isolated $Cu_i$ species ($Cu_i-Cu_i$). Considering that the closest Cu−Cu distances for $Cu_b-Cu_b$ = 11.97 Å, $Cu_b-Cu_i$ = 7.20 Å, and $Cu_i-Cu_i$ = 6.90 Å, respectively, one would expect only very weak antiferromagnetic effects mostly due to the $Cu_b-Cu_i$ and $Cu_i-Cu_i$ interactions. Indeed, this was confirmed by the very low value of the $\theta$ parameter ($\theta$ = 0.4 K, Table 3), as well as by the virtually linear type of the $\chi_m = f(1/T)$ plot (Figure 6, trace a). With the use of the same arguments, the closest Cu−Cu distances in **2**, $Cu_b-Cu_b$ = 8.95 Å, $Cu_b-Cu_i$ = 6.48 Å, and $Cu_i-Cu_i$ = 7.22 Å, respectively, indicated very similar weak antiferromagnetic interactions, which was confirmed experimentally ($\theta$ = 0.4 K; Table 3 and Figure 2a). In **3**, the distances between the two bridging $Cu^{2+}$ atoms within the chains are shorter, $Cu_b-Cu_b$ = 4.75 Å ($Cu_b-Cu_i$ = 6.48 Å and $Cu_i-Cu_i$ = 7.22 Å), which leads to slightly stronger interactions with $\theta$ = 0.8 K

**Table 3.** Final Parameters for the Molar Magnetic Susceptibility Fit of **1**−**5** Using the Curie−Weiss Law $\chi_m = A + C/(T + \theta)$

| | compound | | | | |
|---|---|---|---|---|---|
| | **1** | **2** | **3** | **4** | **5** |
| $A$ (cm$^3$/mol) | $-9.41 \times 10^{-4}$ | $3.85 \times 10^{-2}$ | $-2.79 \times 10^{-4}$ | $2.49 \times 10^{-3}$ | $9.61 \times 10^{-4}$ |
| $C$ (cm$^3$ K/mol) | 1.55 | 0.91 | 0.59 | 2.15 | 1.20 |
| $\theta$ (K) | 0.4 | 0.4 | 0.8 | 5.5 | 7.1 |
| $R_{corr}$ | 0.999 | 0.999 | 0.999 | 0.999 | 0.999 |
| $\mu_{eff}$ (Cu), ($\mu_B$) | 1.81 | 1.55 | 1.55 | 1.57 | 1.09 |
| spin (Cu) | 0.53 | 0.42 | 0.43 | 0.42 | 0.24 |

(Table 3 and Figure 3a). In **4**, there are four $Cu^{2+}$ species within the chains, two bridging and two terminal ($Cu_t$), with shorter distances of $Cu_b-Cu_b = 8.94$ Å, $Cu_b-Cu_t = 5.33$ Å, and $Cu_t-Cu_t = 4.69$ Å, respectively. This indicates stronger, although still weak antiferromagnetic interactions ($\theta = 5.5$ K, Table 3), mostly as a contribution from $Cu_b-Cu_t$ and $Cu_t-Cu_t$ coupling. The magnetic properties of **5** were of particular interest since the data allowed us to resolve the structural disorder described previously (Figure 5b). In all three cases, the $Cu_b-Cu_b$ distances are the same, 8.94 Å, too long to contribute to the overall Cu−Cu interactions. If we consider the first of the three possible orientations of the two disordered $[Cu(NH_3)_3]$ species, i.e., $[Cu(NH_3)_3]_2$ dimers (Figure 5a), the Cu−Cu distance is only 2.72 Å, which by default should lead to very strong interactions. Our experimental measurements, however, yielded a value of $\theta = 7.1$ K, which is of the same magnitude as that in the case of the ordered phase **4**. The distances of $Cu_t-Cu_t = 4.60$ Å and $Cu_b-Cu_t = 5.30$ Å in the orientation shown in Figure 5b are just slightly shorter compared with the ones in **4**, predicting a slightly higher value of $\theta$, which indeed has been observed. Finally, in the orientation shown in Figure 5c, the corresponding distances are $Cu_t-Cu_t = 5.34$ Å and $Cu_b-Cu_t = 5.30$ Å, i.e., slightly longer than the ones in **4**, which would require a slightly lower value of $\theta$. All of the above considerations lead us to conclude that the actual orientation of the disordered $[Cu(NH_3)_3]$ species is the one shown in Figure 5b.

## Discussion

Generally, the synthesis mixtures for **1**−**5** upon preparation had starting pH's >10. In the crystalline products of **1** and **2**, we obtain diprotonated clusters $[H_2Nb_6O_{19}]^{6-}$, and the crystalline products of **3**−**5**, feature nonprotonated clusters $[Nb_6O_{19}]^{8-}$. There are several aspects of the synthetic conditions that can influence protonation of the cluster, including pH and solution polarity. Solution polarity decreases upon the addition of a nonaqueous liquid such as an alcohol, which favors crystallization of salts featuring $[H_2Nb_6O_{19}]^{6-}$, as observed prior.[6] Presumably, more ion pairing between $H^+$ and $[Nb_6O_{19}]^{8-}$ in less-polar solutions increases the population of $[H_2Nb_6O_{19}]^{6-}$. In the case of the crystallization of **1**−**3**, methanol was added to improve the crystallinity of the product, which may have played a role in the protonation of the clusters of **1** and **2**. For all of these syntheses, the Rb salt of hexaniobate was used as a reactant. We have observed that Rb salts of hexaniobate produce more acidic aqueous solutions than the analogous Li, Na, K, or Cs salts. Along with this observation, $^{17}O$ NMR shows an increase in $CO_3^{2-}$ concentration in the Rb salt solutions relative to that of other alkali salt solutions, which is likely responsible for the decrease in pH. Since **1**−**5** are obtained via crystallization in air, adsorption of $CO_2$ may result in decreased pH in some cases and thus influence the formation of protonated clusters $[H_2Nb_6O_{19}]^{6-}$. Finally, crystal packing between lattice components may also influence protonation of the cluster, as the protonated faces of the $[H_2Nb_6O_{19}]^{6-}$ clusters tend to H bond to one another, as previously observed for alkali salts,[6] as well as in **1** and **2**.

The variety of structural and compositional features of the above examples **1**−**5** illustrates the diversity of polyoxoniobate-based materials that can be achieved by introducing different metal or complex cations as linkers and/or charge-compensating species.

Both structural and solution studies of $[Nb_6O_{19}]$ show the bridging oxygen atoms $O_b$ to be the most basic and reactive. Examples include protonation in the solid state on the bridging oxygens[6,12] and transition-metal coordination to bridging oxygens.[4,8] $^{17}O$ NMR studies show that the bridging oxygens are more labile than the terminal oxygens in aqueous solutions of $[Nb_6O_{19}]$,[13] and the reactivity increases with increasing protonation (decreased pH). Structures **1**−**5** reported here are consistent with these studies, featuring both protonated bridging oxygens (**1** and **2**) and Cu bonding predominantly to the bridging oxygen sites (**1**−**5**), both features resulting in distortion of the $[Nb_6O_{19}]$ clusters. Generally, the protonated bridging oxygens, $O_bH$, have $Nb-O_b$ bond lengths of around 2.05−2.15 Å. Trans to these elongated $Nb-O_b$ bonds are shortened $Nb-O_b$ bonds, around 1.91−1.92 Å in length. This same distortion is observed in alkali salts of $[HNb_6O_{19}]^{7-}$ and $[H_2Nb_6O_{19}]^{6-}$.[6] Similarly, the $O_b$ oxygens bonded to linking copper atoms have slightly elongated $Nb-O_b$ bonds of around 2.05 Å and the trans $Nb-O_b$ has a corresponding shortening to around 1.94−1.95 Å. This is similar to the distortion observed in other transition-metal complexes of $[Nb_6O_{19}]$ such as $Mn[Nb_6O_{19}]_2$.[4a]

The type of $CuL_x$ complexes also affects the type of the bonding-oxygen sites (bridging $O_b$ or terminal $O_t$) from the $[Nb_6O_{19}]$ clusters. In **1** and **2**, the linking takes place via two $O_b$ atoms of two adjacent clusters (Figures 1a and 2a).

(12) Ozeki, T.; Yamase, T.; Naruke, H.; Sasaki, Y. *Bull. Chem. Soc. Jpn.* **1994**, *67*, 3249.

(13) (a) Filowitz, M.; Ho, R. K. C.; Klemperer, W. G.; Shum, W. *Inorg. Chem.* **1979**, *18*, 93. (b) Alam, T.; Nyman, M.; Cherry, B. R.; Segall, J. M.; Lybarger, L. E. *J. Am. Chem. Soc.* **2004**, *126*, 5610. (c) Black, J.; Nyman, M.; Casey, W. H. *J. Am. Chem. Soc.* **2006**, *128*, 14712.

The two protonated sites and the specific geometry of the chains (dimers) likely prevent the attachment of additional $[Cu(en)_2]$ complexes in both cases. In **3**, each pair of $[Cu(NH_3)]$ linkers spanning two clusters is connected to a pair of $O_b$ from one $[Nb_6O_{19}]$ cluster and to a single $O_t$ from a neighboring $[Nb_6O_{19}]$ cluster (Figure 3). For structures **4** and **5**, although the decorating copper cations are bonded to the cluster faces via three $O_b$ oxygens, the linking copper cations are only bonded to terminal oxygen atoms $O_t$. In no case do we observe a copper cation linking two faces of neighboring $[Nb_6O_{19}]$ clusters via $\mu_3$ bonding, as is the case in the Mn/Ni$[Nb_6O_{19}]_2$ dimers.[4a] This suggests that a more open linking mode resulting from bonding to terminal oxygen atoms is necessary for propagating an infinite network.

Clearly, the different number of copper linkers in **1**−**5** is determined by the different nature and size of the ligands used. In the cases involving the bigger en ligand, **1** and **2**, it is geometrically impossible to "squeeze" more that one $[Cu(en)_2]$ complex between the $[Nb_6O_{19}]$ clusters to form additional Cu−O−Nb bonds. In contrast, the much smaller $NH_3$ and $H_2O$ ligands provide variable ways of linking that lead to phases containing two and even four copper atoms per $[Nb_6O_{19}]$ cluster, as demonstrated in the cases of **3**−**5**.

The nature of the metal complexes also affects the resulting overall structures. The use of the Jahn−Teller distorted $Cu^{2+}$ metal centers provides two elongated axial bonds that link two adjacent $[Nb_6O_{19}]$ clusters, as illustrated in **1** and **2**. The use of the more symmetrical transition-metal ion $Co^{2+}$, however, does not provide for such a fortunate opportunity. Thus, in our attempt to synthesize a series of extended $[Nb_6O_{19}]$−$Co(en)_x$- and $[Nb_6O_{19}]$−$Co(NH_3)_x$-type structures similar to **1**−**5**, we obtained two isolated ionic cluster-type phases, $[Co(en)_3]_3[Nb_6O_{19}H_2]\cdot 10H_2O$ (**6**) and $[Co(NH_3)_6]_3[Nb_6O_{19}H_2]$ (**7**).[14] Similar phases have been previously characterized, but no crystal structures have been reported.[15] Both phases can be described as isolated $[Nb_6O_{19}H_2]^{6-}$ clusters symmetrically diluted by $[Co(en)_3]^{2+}$ and $H_2O$ in **6** and by $[Co(NH_3)_6]^{2+}$ in **7**, respectively (Supporting Information, Figure SI1). In contrast to the Ni− and Mn−$[Nb_6O_{19}]$ phases discussed in the Introduction, the $[CoL_6]$ complexes do not associate at all with the $[Nb_6O_{19}]$ clusters by the decorating or the linking motifs.

The overall charge of the chains (dimers) in **1**−**5** varies as a function of $CuL_x$ linkers and $CuL_x$ decorations. The dimers in **1** are of 10− charge while their one-dimensional extension in **2** reduces the chains' charge to 4−. In a similar way, the charge of the chains in **3** is 4−, while the addition of two more decorating Cu-complexes in **4** and **5** reduces the charge to zero.

In contrast to most of the polyoxoniobates known to date, the overall charge balance in **1**−**7** is provided not only by alkali cations but also by charged $[ML_x]^{2+}$ (M = Cu, Co) complexes, as well. In some cases, the countercations are mixed, $Rb^+$ and $[Cu(en)_2(H_2O)_2]^{2+}$ in **1** and $Rb^+$, $[Cu(NH_3)_2(H_2O)_4]^{2+}$, and $[Cu(NH_3)_4(H_2O)_2]^{2+}$ in **3**. In a similar way, the charge balance in $Cu(en)_2$-linked $[Nb_{24}O_{72}H_9]$ is provided by $[Cu(en)_2(H_2O)_2]^{2+}$ and organic cations $H_2$−$en^{2+}$.[8] In **2**, **6**, and **7**, the charge balance is provided exclusively by charged complexes $[Cu(en)_2(H_2O)_2]^{2+}$, $[Co(en)_3]^{2+}$, and $[Co(NH_3)_6]^{2+}$, respectively.

Due to the zero-charge of the $\{-[Nb_6O_{19}][Cu(L_4)]_4-\}$ chains in **4** and **5**, there are no countercations of any type in these structures. This is certainly unprecedented in polyoxoniobate chemistry, although infinite neutral solids based on Mo−V anionic clusters decorated by transition-metal complexes have been reported.[16] These neutral one-dimensional chains demonstrate the potential for diversification of polyoxoniobate-based materials if the more traditional alkali counterions are replaced by metal complexes or organic cations. It is also noteworthy that dehydration of **4** results in another crystalline phase that retains a long-range order. In both the hydrated and dehydrated phases, the chains are held together by hydrogen bonding among the Cu-bound water molecules and the cluster oxygens with $O_w$−$O_w$ and $O_w$−$O_b$ distances ranging from 2.7 to 3.0 Å.

## Summary

Alkali salts of $[Nb_6O_{19}]^{8-}$ combined with copper amine complexes in aqueous solution under ambient conditions have produced unprecedented one-dimensional phases featuring Cu-linked hexaniobate Lindqvist clusters. We attribute the variety of linked-cluster geometries obtained to the Jahn−Teller distortion of the d-9 $Cu^{2+}$ ion and the diversity of copper ligands employed ($H_2O$, $NH_3$ and en). Anionic chains were charge-balanced by a combination of $Rb^+$ and $CuL_x$ complexes or just $CuL_x$ complexes. Two phases featuring neutral chains were also produced, a phenomenon which had not been previously observed for polyoxoniobate materials. Weak antiferromagnetic coupling was observed in all five reported phases, which was consistent with the closest Cu−Cu distances observed by XRD. Furthermore, the magnetic measurements provided data to resolve Cu disorder in one of the neutral-chain phases.

The hexaniobate Lindqvist ion $[Nb_6O_{19}]^{8-}$ has a high charge density; it is robust and stable under appropriate conditions (pH >10) and very symmetric. These properties together render it an ideal anionic building block for the assembly of complex materials; yet these materials are not formed with Ni, Co, Mn, or Re as cationic linkers. This study has shown that Jahn−Teller distorted $Cu^{2+}$ linkers, on the other hand, *do* favor the assembly of infinite solids based on $[Nb_6O_{19}]^{8-}$ ions. Generally, we suggest that cationic complexes that prefer asymmetric coordination will propagate the formation of infinite solids, whereas more symmetrically coordinated cationic linkers will form decorated monomers or dimers with $[Nb_6O_{19}]^{8-}$ ions.

(14) Both compounds have been synthesized in the same way as described for **1**−**5**: **6**, $[Co(en)_3]_3[Nb_6O_{19}H_2]\cdot 10H_2O$, space group $R\bar{3}c$; $a$ = 18.205 Å, $c$ = 35.719 Å. **7**, $[Co(NH_3)_6]_3[Nb_6O_{19}H_2]$, space group $I23$; $a$ = 14.302 Å.

(15) Flynn, C. M.; Stucky, G. D. *Inorg. Chem.* **1969**, *8*, 178.

(16) Gu, X. J.; Peng, J.; Shi, Z. Y.; Chen, Y. H.; Han, Z.; Wang, E. B.; Ma, J. F.; Hu, N. H. *Inorg. Chim. Acta* **2005**, *358*, 3701.

**Acknowledgment.** Sandia is a multiprogram laboratory operated by the Sandia Corporation, a Lockheed Martin Company, for the United States Department of Energy's National Nuclear Security Administration under Contract DE-AC04-94AL85000. This work was supported by Sandia National Laboratories' Laboratory Directed Research and Development (LDRD) program. We thank Reference Metals, Inc., CBMM, Araxá, Brazil, for the generous gift of hydrous niobia.

**Supporting Information Available:** Crystal data for **1**−**5** in CIF format; PDF file containing a figure illustrating structures **6** and **7**, IR spectra of **1**−**5**, and TGA data for **1**−**5**. This material is available free of charge via the Internet at http://pubs.acs.org.

IC0624118